Scientific Research Publishing

World Journal of Condensed Matter Physics, 2025, 15(1), 1-15
https://www.scirp.org/journal/wjcmp
ISSN Online: 2160-6927
ISSN Print: 2160-6919

On the Remarkable Thermodynamic Properties of the Helical Multiferroic Quantum Spin Chain

Erna Leticia Tchinda Ngounou[1,2], Blaise Ndakom[3], Georges Collince Fouokeng[1,3,4*], Ngarmaim Nadjitonon[3,5], Aurélien Kenfack Jiotsa[1]

[1]Nonlinear and Complex Systems Physics, Department of Physics, Ecole Normale Superieure, University of Yaounde 1, Yaounde, Cameroon
[2]UNESCO-UNISA-iTLABS/NRF Africa Chair in Nano-Sciences and Nanotechnology, CGS, Department of Physics, University of South Africa, Muckleneuk Ridge, Pretoria, South Africa
[3]Laboratoire d'Etude et de Recherche en Techniques Industrielles, Université de N'DJAMENA, N'Djamena, Tchad
[4]Department of Physics, Faculty of Science, Laboratoire de Matière Condensée, d'Electronique et de Traitement de Signal, University of Dschang, Dschang, Cameroon
[5]Laboratoire d'Etude et de Recherche en Techniques Industrielles, Université de Doyaba, Sarh, Tchad
Email: *fouokenggc@yahoo.fr

How to cite this paper: Ngounou, E.L.T., Ndakom, B., Fouokeng, G.C., Nadjitonon, N. and Kenfack Jiotsa, A. (2025) On the Remarkable Thermodynamic Properties of the Helical Multiferroic Quantum Spin Chain. *World Journal of Condensed Matter Physics*, **15**, 1-15.
https://doi.org/10.4236/wjcmp.2025.151001

Received: January 3, 2025
Accepted: February 25, 2025
Published: February 28, 2025

Abstract

The flexibility of magnetoelectric coupling in $RMnO_3$ is enhanced by the sensitivity of such materials to diverse interactions. This complicates the straightforward comprehension of its various physicochemical properties, such as magnetoelectric properties. The present study measures the impact of the simultaneous action of Dzyaloshinsky-Moriya (DM) and Kaplan-Shekhtman-Entin-Wohlman-Aharony (KSEA) interactions on the thermodynamic ability to induce phase transition in a rare-earth (R) Mn perovskite of $TbMnO_3$ (TMO) helical compound at thermal equilibrium using entropy, heat capacity, and magnetoelectric (ME) coupling factor. We found that the behaviour of entropy is similar to that of the ME coupling factor, which emphasizes the metamagnetoelectric properties for ferric transition points of this order. The intrinsic physics of transition points, which is accurately described in terms of entropy, reveals a muddle caused by a rearrangement of magnetic moments. The magnetic rearrangement at the corresponding critical points of entropy shows a different loop than the heat capacity. Under the influence of the DM interaction, the KSEA interaction accelerates the decrease of specific heat and entropy as the ME coupling increases. However, the KSEA interaction reduces transition dynamics and opposes symmetrical inversion caused by DM interaction. The observed thermodynamic capacity changes caused by the simultaneous action of DM and KSEA interactions are the signature of a system attempting

to minimize the possible distortions that are primarily responsible for the loss of quantum property.

Keywords

KSEA Interaction, Thermodynamics, Helical Multiferroics Spin Chain, DM Interaction

1. Introduction

Research on multifunctional systems has received increased attention in solid-state physics over the last decade, with a focus on nanosystems with improved storage capacities and ease of conveying information over long distances with less loss. The various concerns are related to both magnetism and ferroelectricity. This was made possible by the discovery of spin [1] [2], which can be polarised by an external field, resulting in the formation of ME coupling. In recent years, multiferroic materials have gained attention due to their common ferric order (ferroelectric, ferromagnetic, ferroelastic, ferrotoroidic, and antiferromagnetic). These materials can switch polarization, magnetization, and strain between symmetric or opposite values under external fields or mechanical stresses [3]. That is, each field or mechanical stress is thermodynamically conjugated to ferroelectricity, ferromagnetism, and ferroelasticity, respectively [4]-[6]. Furthermore, multiferroic materials have been the subject of much more theoretical [7] [8] and experimental studies [9]-[12] in recent years, with a particular emphasis on how to handle an existing coupling between different ferric orders. Controlling ferroic order enables new technological applications in magnetic storage (stable memories), sensors [13], spintronics [14], and nanotechnologies [15]. The multiferroic materials with spin-1/2 chains model under the ME coupling have been theoretically investigated [16] [17] with spin-current mechanism in a model with electric ordering [18].

Regardless of their origin, magnetism and ferroelectric order coexist in these materials at the same temperature [19]. The partially filled "*d*" or "*f*" shell of transition metals, where the interaction between localized moments exhibits magnetic properties, is typically responsible for the microscopic magnetism that exists, while the charge orderings, lone pair, etc., are responsible for the ferroelectric order, where the "*d*" shell is completely devoid of electrons in contrast to magnetism [20] [21]. Multiferroic materials exhibit remarkably strong couplings between charges, spins, crystal lattice, and orbital degrees of freedom, making them ideal candidates for developing novel devices for a variety of quantum technology applications. Many authors have demonstrated that in ME systems, two transitional phases occur at the same critical temperature, with the coupling between ferroelectricity and ferromagnetism being typically and strongly enhanced at the lower temperature phase transition [22] [23].

Since the discovery of the giant ME coupling effect in $TbMnO_3$ (TMO), multiferroic manganite $RMnO_3$ (where R is a rare-earth element) that hosts an intimately coupled ferroelectrics (FE) and magnetic order has attracted significant attention in the development of new devices with multifunctionality [13]. One of the most common causes of multiferroicity is the inverse DM interaction between adjacent spins. Experimental and theoretical studies on multiferroic $BiFeO_3$ and $RMnO_3$ (R = Tb, Dy, and Y) compounds have included the Single Ion Anisotropy (SIA) and spin-orbit coupling interaction in the frustrated spin Hamiltonian [24]-[26]. Recently, research into the $TbMnO_3$ compound has revealed an intriguing helical magnetic structure for the most likely candidates to host ferroelectricity [26] in contrast to the $LaMnO_3$ properties, where the single-occupied eg orbitals with antiferro-type ordering imply a ferromagnetic nearest-neighbour (NN) interaction, in the $TbMnO_3$, a sizeable overlap of the eg orbitals of the next nearest-neighbour (NNN) sites along "*b*" appears from a large c-axis octahedron rotation [27], giving rise to a strong NNN antiferromagnetic interaction [14]. The overlap of NNN's, e.g., orbitals, which define ferromagnetic order well in the "*ab*" planes, is strongly frustrated, resulting in complex magnetic ordering. Due to the absence of conventional magnetic order [28] [29], those compounds' ferroelectricity below about 8K was their primary selling point. This phenomenon has been linked to the emergence of the inverse DM mechanism [18] [20].

In Refs [26] [30]-[32], the classical isotropic model with frustrated spin arrangement leading to a helical spin arrangement was investigated using numerical simulation and experiments that demonstrated the interplay of several interactions. In fact, a spin chain that includes an antiferromagnetic NNN interaction as well as a ferromagnetic exchange interaction between NN spins is frustrating [26] [33]. The NNN interaction frustration results in a helical spin structure with a pitch angle determined by the ratio (J and J' represents the NN and NNN exchange couplings, respectively). However, despite the fact that the symmetric and antisymmetric exchange couplings are rigorously determined experimentally or estimated from simulations using the lattice parameters, they may differ under certain conditions. Recent research has shown that rare-earth-metal (R) Mn perovskites, $RMnO_3$ (R = Tb, Dy, and Y), are well suited to elucidate magnetoelectric excitations because the polarization in the ferroelectric phase is significant and the magnetoelectric coupling is remarkably large [14].

In this paper, we investigated the simultaneous action of DM and KSEA interactions on the thermodynamic properties and on the ME coupling of a proposed model of $RMnO_3$ (R = Tb) multiferroic with helical frustrated spin chains, where the NN interactions are ferromagnetic and the NNN antiferromagnetic and driven by an external electric field. The considered action is to toke to improve the behaviour of entropy, heat capacity and the ME coupling factor. The KSEA interactions which actions oppose the symmetric inversion caused by DM interactions are used to control the dynamics of transition phases induced by DM interactions. The observed contributions would be significant in the process of forming and controlling different phases in multiferroics, which is important in spintronics.

2. Model and Theoretical Formulation

This section presents the theoretical approach to determine the thermodynamic properties and the ME coupling factor of the $TbMnO_3$ multiferroic system model, subjected to an external electric field constraint, while considering the simultaneous action of DM and KSEA interaction [32] [34].

$$H = H_{ex} + H_z + H_{SIA} + H_{Pol} + H_{DM} + H_{KSEA} \tag{1}$$

The above Hamiltonian is decomposed as follows:

$$H_{ex} = \sum_i \left(J_x S_i^x S_{i+1}^x + J_y S_i^y S_{i+1}^y \right) + \sum_i \left(J_x' S_i^x S_{i+2}^x + J_y' S_i^y S_{i+2}^y \right) \tag{2}$$

The system spin-exchanges term, where, J_x, J_x' and J_y, J_y' are the components of the coupling factors in the *x*- and *y*-direction respectively,

$$H_Z = -\Omega \sum_i S_i^z \tag{3}$$

the Zeeman energy with $\Omega = g\mu_B \lambda$ the transverse magnetic field in unit of energy (respectively with the g-factor $g = 2$ in the present work, μ_B the Bohr magneton and λ the magnetic field in Tesla),

$$H_{SIA} = -\Delta \sum_i \left(S_i^z \right)^2 + K \sum_i \left(\left(S_i^x \right)^2 - \left(S_i^y \right)^2 \right) \tag{4}$$

the contribution of the single-ion anisotropy in the three directions of space given by the wave function of the occupied orbital [23]. This term is governed by both magnetocrystalline constants Δ and K that render the magnetization along the *z*-direction.

$$H_{POL} = -\mathbf{E} \cdot \mathbf{P} \tag{5}$$

is the interaction part of the external electric field $\mathbf{E}(0, E, 0)$ with the induced electric polarization $\mathbf{P} = \pi_{i,i+1} \sum_i \mathbf{e}_x \times \left(\mathbf{S}_i \times \mathbf{S}_{i+1} \right)$ in the spin-chain. $\pi_{i,i+1}$ is the factor inducing the modulation of the polarization term which is calculated from the lattice parameter and expressed in unit energy [35].

$$H_{DM} = D \sum_i \left(S_i^y S_{i+1}^x - S_i^x S_{i+1}^y \right) \tag{6}$$

denotes the contribution of the DM interaction (with D the DM parameter taken along the *z*-direction), due to the antisymmetric exchange interactions of spins in the plane. For large-S limit, the DM favors non-collinear spin spirals and induces spin-current-driven polarization via inverse DM mechanism.

$$H_{KSEA} = \Gamma_z \sum_i \left(S_i^x S_{i+1}^y + S_i^y S_{i+1}^x \right) \tag{7}$$

is the KSEA interaction term, which in the semiclassical regime limit, adds symmetric anisotropy, modifying the spiral's pitch and gap, and renormalizes spin-wave velocities and electromagnon energies. For the fact that the KSEA interaction does not have a fixed special point, but depends on the point of intersections in a certain numerical and relatively dense in value range, and sparse in other numerical value ranges, we consider Γ_z such that the symmetric anisotropy KSEA interaction is taken along the z-direction. The sum is over the sites $i \in]0, N[$; N being the number of spins per unit volume.

The beginning stage for computing the thermodynamic functions is the calculation of the energy spectrum of the proposed model. This can be accomplished from the spin-wave approximation method with the spin operators expressed in terms of Pauli matrices $\tilde{\mathbf{S}}_i = \hbar 2\tilde{\sigma}_i$, by referring to the strongly reduced moment Mn revealed in the neutron-scattering experiment [31]. $\sigma_i^{\alpha}\left(\alpha = x, y, z\right)$ denotes the three Pauli matrices at site i. This leads to the dispersion relation as free fermions' energy spectrum

$$\omega_q = \sqrt{\left(\frac{J_x + J_y}{2}\cos\left(q\right) - \frac{J_x' + J_y'}{2}\cos\left(2q\right) + \left(D - \pi_{i,i+1}E\right)\sin\left(q\right) - \Omega\right)^2 + \left(\Gamma_z \sin\left(q\right)\right)^2}$$

In this paper, depending on the $TbMnO_3$ material, we deal with isotropic exchange interactions of NN ferromagnetic ($J_x = J_y = -0.79$ meV) and of NNN antiferromagnetic ($J_x' = J_y' = 0.62$ meV). The model Hamiltonian in Equation (1) is mapped in the spin-wave approximation to be compared to usual quantum gases which are conveniently treated using the canonical set [3] [36]. Since $TbMnO_3$ has non-collinear spin order and Mn^{3+} has $S = 2 \gg -1/2$, quantum fluctuations are weaker, making the spin-wave approximation is used for modelling its magnon spectrum.

$$H = \sum_q \omega_q \left(\eta_{-q}^{+}\eta_q - \frac{1}{2}\right) - \frac{N}{2}\left(\frac{\Delta}{2} + \Omega\right) \tag{8}$$

where η are Bogoliubov quasiparticles expressed in terms of Fourier transform operator $c_q = \sigma_i^{-}\left[\prod_{j \le i-1}\left(-\sigma_j^z\right)\right]$ and wave numbers taking in the range $\pi \le q \le -\pi$.

Within the Fermi-Dirac statistical theory, the thermodynamic parameters and the magnetoelectric coupling factor are calculated in the spin-wave approximation using the partition function associated with Hamiltonian Equation (8) given by:

$$\begin{aligned} Z &= Tr\exp\left\{-H\cdot\Theta\right\} \\ &= \exp\left\{\frac{N\Theta}{2}\left(\frac{\Delta}{2} + \Omega\right)\right\}\prod_q \exp\left(\frac{\Theta\cdot\omega_q}{2}\right)\prod_q\left(1 + \exp\left(-\Theta\cdot\omega_q\right)\right) \end{aligned} \tag{9}$$

from which the free energy is defined as

$$F = -T\ln Z = -T\left(\frac{N\Theta}{2}\left(\frac{\Delta}{2} + \Omega\right) - \frac{\Theta}{2}\sum_q \omega_q\right) - \frac{1}{\Theta}\sum_q \ln\left(1 + \exp\left(-\Theta\cdot\omega_q\right)\right) \tag{10}$$

where T is the absolute temperature, K_B the Boltzman constant and $\Theta = 1/K_B T$.

From Equation (10), the thermodynamic parameters and the magnetoelectric coupling factor can be evaluated.

3. Thermodynamic Properties and Magnetoelectric Coupling Factors

This section evaluates the Boltzmann entropy, specific heat capacity, and ME coupling factor in order to demonstrate the influence of the simultaneous KSEA and DM interactions on the thermodynamic properties and on the metamagnetoelectric

transition of the system under study. The thermodynamic properties of quantum materials can be found in the canonical distribution using the statistical sum Equation (9) to highlight the influence of the simultaneous effect of DM and KSEA on a helical spin chain system subjected to an external electric field constraint made from $TbMnO_3$(TMO) multiferroic compound.

3.1. Entropy

At thermal equilibrium, the Boltzmann entropy at constant volume can be expressed in terms of the Helmholtz free energy F as:

$$S = -\frac{\partial F}{\partial T} = K_B \sum_q \ln\left(1+\exp\left(-\Theta\cdot\omega_q\right)\right) + \frac{1}{T}\sum_q \frac{\omega_q}{\left(1+\exp\left(\Theta\cdot\omega_q\right)\right)} \tag{11}$$

with the numerical representation of the behavior in (Figure 1) to (Figure 5), showing how juxtaposed KSEA interactions on DM interactions can be used to better preserve the stability of the system.

The temperature-dependent entropy (Figure 1) and the entropy variations of the fields (electric and magnetic) for different values of DM and KSEA parameters (Figures 2-5) can be compared to the results obtained previously in [3]. In Figure 2 and Figure 3, the entropy shows curvy behaviour with a latency interval (transition time). It is the time it takes for the system to transition from the ferromagnetic to the antiferromagnetic phase and back again. This latency becomes more noticeable when the study is conducted in accordance with the magnetic field variation shown in Figure 3. We discovered that when the combined effect of DM and KSEA is taken into account, the $TbMnO_3$ compound's plotted curves decrease more quickly than when only the DM interaction is taken into account [3]. These findings indicate that when the simultaneous effect of DM and KSEA interactions is considered, the latency time interval, and curvy behaviour increase. This demonstrates that when designing storage memories in the strong magnetic field regime, it is advisable to consider the simultaneous influence of DM and KSEA interactions.

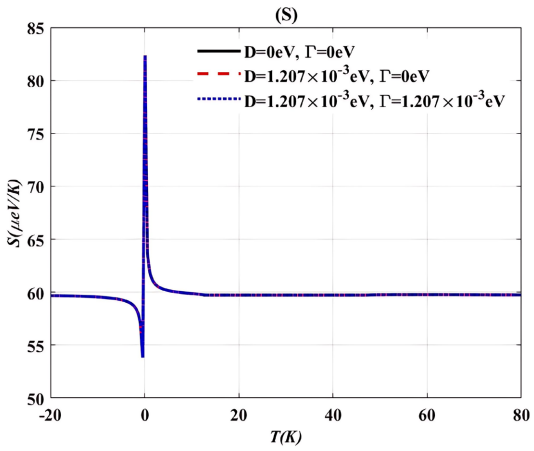

Figure 1. Temperature's dependence of entropy for different values of DM and KSEA interactions, considering the magnetic field and the electric field intensity to be $\lambda = 0.5$ T and $E = 0.3$ V/m .

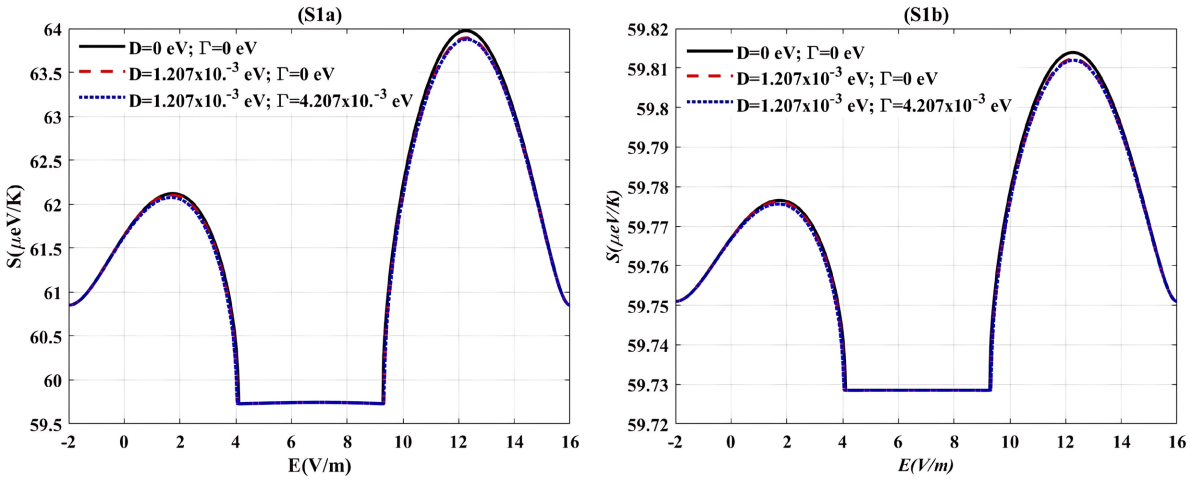

Figure 2. Electric field's dependences of Entropy for different values of DM and KSEA interactions, considering the magnetic field intensity to be $\lambda = 0.1\,\mathrm{T}$. (S1a) $T = 1\,\mathrm{K}$ and (S1b) $T = 50\,\mathrm{K}$.

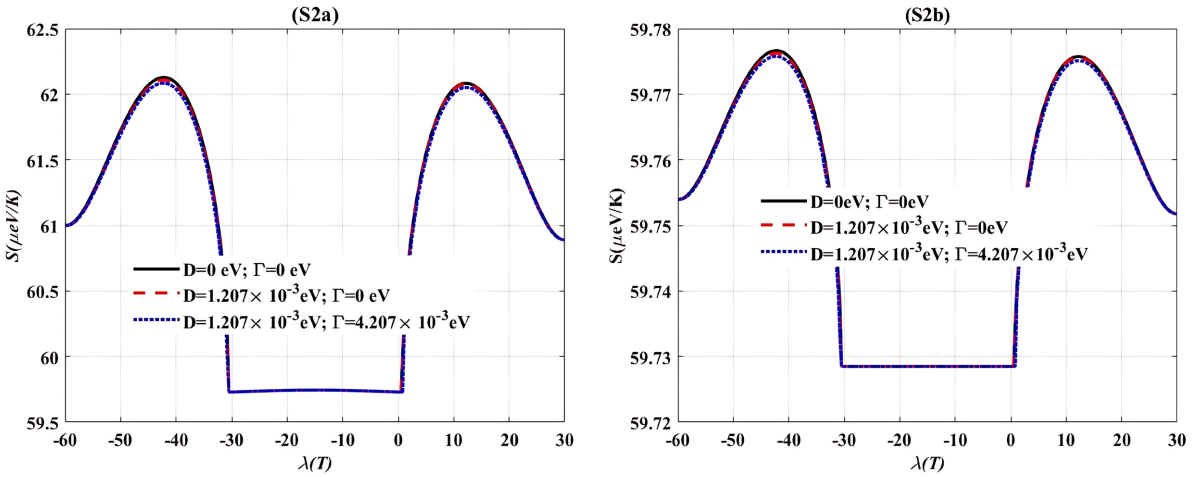

Figure 3. Magnetic field's dependence of Entropy for different values of DM and KSEA interactions, considering the electric field intensity to be $E = 0.3\,\mathrm{V/m}$. (S2a) $T = 1\,\mathrm{K}$ and (S2b) $T = 50\,\mathrm{K}$.

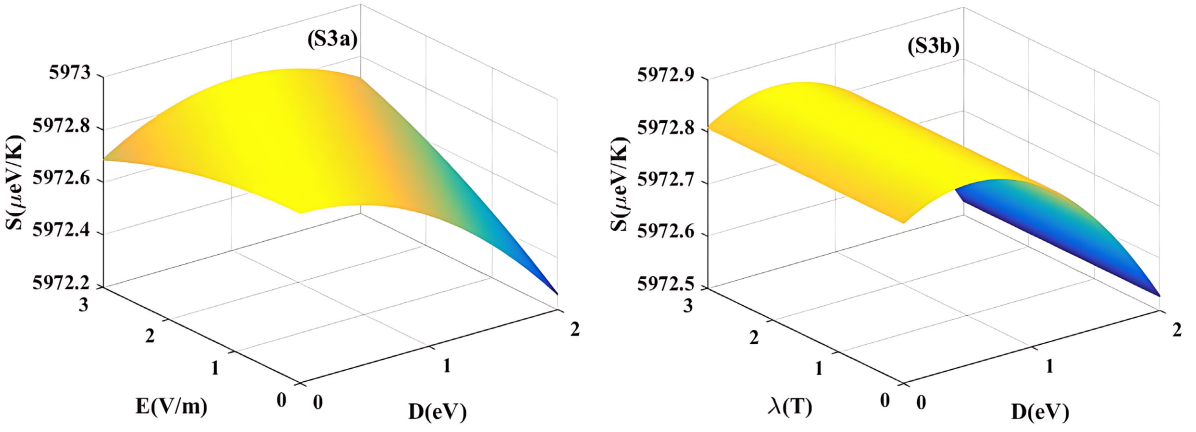

Figure 4. 3D variation of the entropy with DM interaction and external (S3a) electric field (with $\lambda = 1.5\,\mathrm{T}$) and (S3b) magnetic field (with $E = 0.5\,\mathrm{V/m}$). $\Gamma_z = 1.207\times10^{-3}\,\mathrm{eV}$ and $T = 100\,\mathrm{K}$.

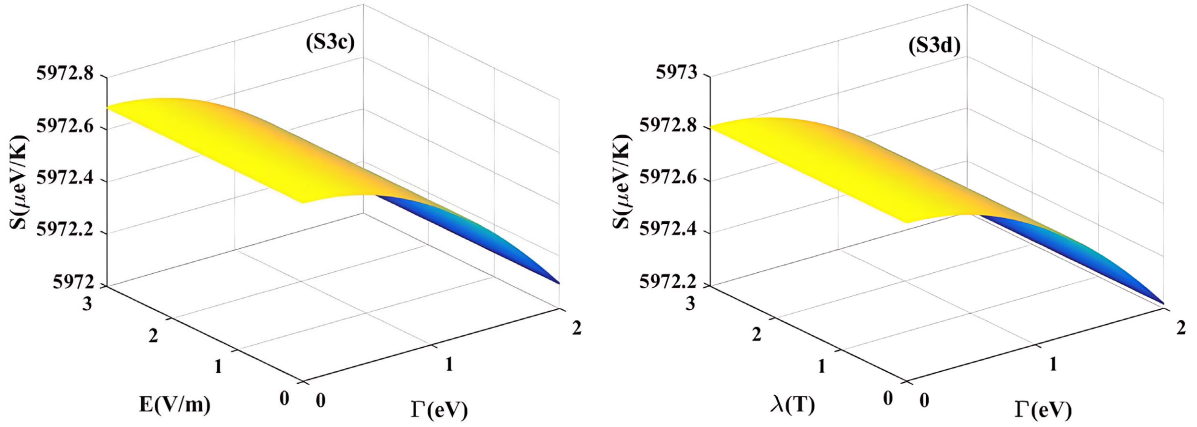

Figure 5. 3D variation of the entropy with KSEA interaction and external (S3c) electric field (with $\lambda = 1.5$ T) and (S3d) magnetic field (with $E = 0.5$ V/m). $\Gamma_z = 1.207 \times 10^{-3}$ eV and $T = 100$ K.

3.2. Heat Capacity

Consequently, from Equation (11), the specific heat capacity is obtained as:

$$C_v = T\frac{\partial S}{\partial T} = \frac{\Theta}{T}\sum_q \omega_q^2 \cdot \frac{\exp\left(\Theta \cdot \omega_q\right)}{\left(1+\exp\left(\Theta \cdot \omega_q\right)\right)^2} \tag{12}$$

which is a function of temperature, the external fields as well as the DM and KSEA interactions.

In terms of entropy, to characterize the effect of transitions in the system, the heat capacity is investigated as a function of temperature in **Figure 6**, of electric in **Figure 7**, and of magnetic field in **Figure 8**. Additionally, we plotted the specific heat capacity in three dimensions in **Figure 9(C3a)** with an electric field and DM factor, and in **Figure 9(C3b)** with a magnetic field and DM factor.

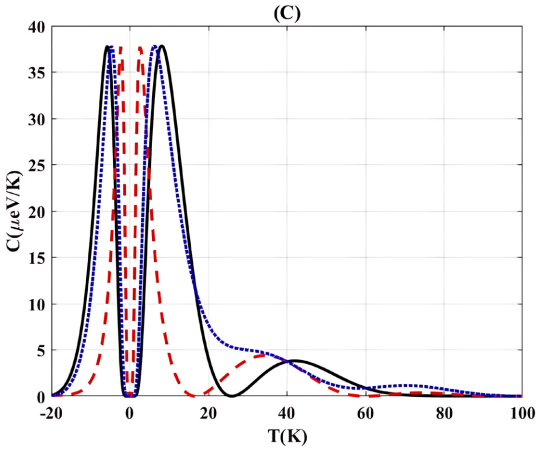

Figure 6. Temperature's dependence on the specific heat capacity plotted considering different values of DM and KSEA interactions to be $D = 0$ eV and $\Gamma = 0$ eV for the curve in black colour; $D = 1.207 \times 10^{-3}$ eV and $\Gamma = 0$ eV for the curve in red colour; $D = 1.207 \times 10^{-3}$ eV and $\Gamma = 1.207 \times 10^{-3}$ eV for the curve with blue colour. The other parameters are: $\lambda = 0.5$ T and $E = 0.3$ V/m.

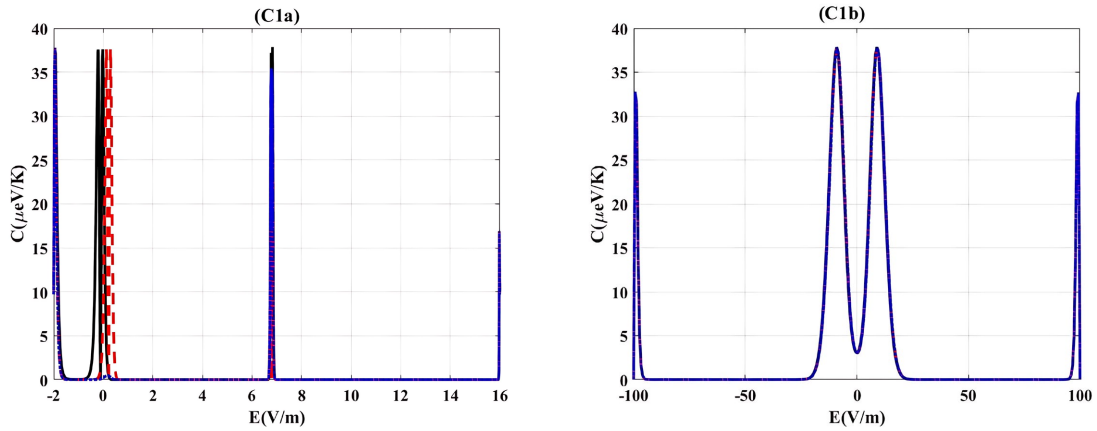

Figure 7. Electric field's dependence on the specific heat capacity plotted considering different values of DM and KSEA interactions to be $D=0\,\text{eV}$ and $\Gamma=0\,\text{eV}$ for the curve in black colour; $D=1.207\times10^{-3}\,\text{eV}$ and $\Gamma=0\,\text{eV}$ for the curve in red colour; $D=1.207\times10^{-3}\,\text{eV}$ and $\Gamma=1.207\times10^{-3}\,\text{eV}$ for the curve with blue colour respectively with (C1a) $T=1\,\text{K}$ and (C1b) $T=50\,\text{K}$. The magnetic field intensity is chosen to be $\lambda=2\,\text{T}$.

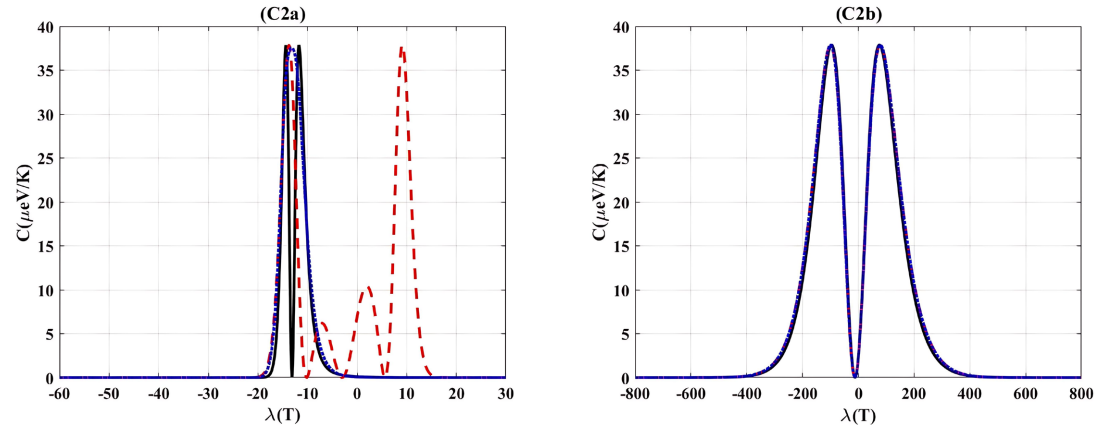

Figure 8. Magnetic field's dependence on the specific heat capacity plotted considering different values of DM and KSEA interactions to be $D=0\,\text{eV}$ and $\Gamma=0\,\text{eV}$ for the curve in black colour; $D=1.207\times10^{-3}\,\text{eV}$ and $\Gamma=0\,\text{eV}$ for the curve in red colour; $D=1.207\times10^{-3}\,\text{eV}$ and $\Gamma=1.207\times10^{-3}\,\text{eV}$ for the curve with blue colour respectively with (C1a) $T=1\,\text{K}$ and (C1b) $T=50\,\text{K}$. The electric field intensity is chosen to be $E=0.3\,\text{V/m}$.

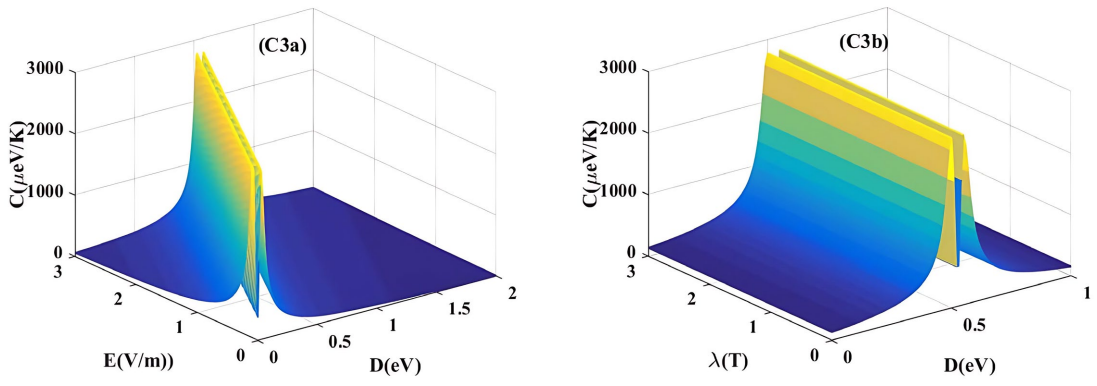

Figure 9. 3D variation of specific heat with DM interaction and external (C3a) electric field (with $\lambda=1.5\,\text{T}$) and (C3b) magnetic field (with $E=0.5\,\text{V/m}$). $\Gamma_z=1.207\times10^{-3}\,\text{eV}$ and $T=100\,\text{K}$.

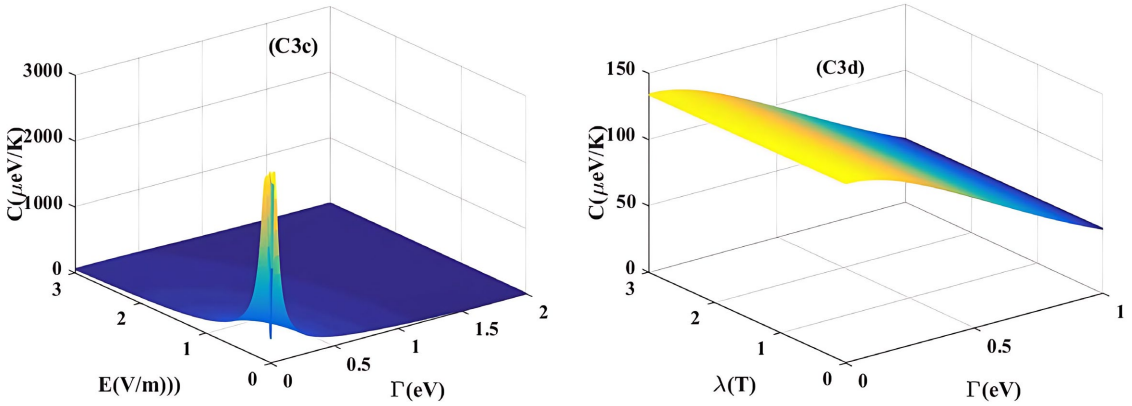

Figure 10. 3D variation of specific heat with KSEA interaction and external (C3c) electric field (with $\lambda = 1.5$ T) and (C3d) magnetic field (with $E = 0.5$ V/m). $\Gamma_z = 1.207 \times 10^{-3}$ eV and $T = 100$ K.

Quantum phase transitions mean transitions at $T = 0$. However, the transition points are highlighted by peak-like behaviours around them. **Figures 1-10** show sudden deft and sudden bird movements around critical temperature and field points. Another result of this research is that a shift observed at different transition points caused by a DM interaction factor to variations in temperature **Figure 1** and **Figure 6** and fields **Figure 2**, **Figure 3**, **Figure 7**, and **Figure 8** are flattened under the influence of KSEA interactions. We can conclude that by tuning a non-temperature parameter, specifically cumulating DM with KSEA interactions, we can control a transition temperature such as the Curie or Néel temperature. The electric field dependence of entropy and specific heat is nonlinear and anharmonic (see **Figure 2** and **Figure 7**), whereas the magnetic field dependence is nonlinear but maintains harmonicity in the distribution of vibrational modes (see **Figure 3** and **Figure 8**).

The anharmonic behaviour caused by the electric field and supported by the temperature distribution is indicative of a transition to ferroelectric order, whereas the magnetic field causes nonlinearity with harmonic modes, which is maintained by DM and KSEA interactions. The various harmonic modes form optimal magnetic domains for information storage. The antisymmetric property of DM interaction allows it to create information transmission dynamics, increasing its amplitude while maintaining its width. The KSEA interaction embodies the symmetrical property, allowing it to improve both the amplitude and width of the signal during transmission. The increase in width here allows the information to be kept as long as possible in the phase preceding the transition. It is clear that the combined effect of DM and KSEA interactions plays an important role in information control in hexagonal multiferroics.

4. Influence of the KSEA Interaction on the Linear ME Coupling Factor

The new challenge in solid-state physics is to find new multifunctional materials with a strong ME coupling factor. Following recent research in solid-state materials,

multiferroic materials with linear ME coupling have been found to be a candidate of choice [4] [37]. The linear ME coupling in class II multiferroics system is obtained through magnetization or polarization and particularly exhibits the same response of the system under electric or magnetic field excitation with an intriguing survival of the ferroelectric order when the ferromagnetism is dropped, allowing the ferric order separation in such a magnetoelectric system. The significant insight is that, thermodynamically, the coexistence of the magnetic-electric phase in a ferroelectric material with SIA and DM interaction induces a magnetoelectric effect [3] [23] [37]. Why should the contribution of KSEA interaction be juxtaposed to that of DM? The answer to this question is related to the same method used in [36] we also got the same result in Equation (13), plotted respectively in **Figures 11-13**,

$$\begin{aligned}\alpha &= \frac{\partial P}{\partial \Omega} = \frac{\partial M}{\partial E} \\ &= \pi_{I,I+1}\Omega/\lambda \sum_q \left(\frac{\sin q}{\omega_q} - \frac{\left(J\cos q - J'\cos 2q + \left(D - \pi_{I,I+1}E\right)\sin q - \Omega\right)^2 \cdot \sin q}{\omega_q^3} \right)\left(\frac{1}{2} - \frac{1}{1+\exp\left(\Theta\cdot\omega_q\right)} \right) \\ &+ \frac{\pi_{I,I+1}\Omega\cdot\Theta}{\lambda} \sum_q \left(\frac{\left(J\cos q - J'\cos 2q + \left(D - \pi_{I,I+1}E\right)\sin q - \Omega\right)^2 \cdot \sin q}{\omega_q^2} \left(\frac{\exp\left(\Theta\cdot\omega_q\right)}{\left(1+\exp\left(\Theta\cdot\omega_q\right)\right)^2} \right) \right)\end{aligned} \quad (13)$$

From the various graphs obtained, we obtain a definite improvement in the magnitude of the ME coupling factor under the simultaneous effect of the two interactions (DM and KSEA). This gives rise to the control of metamagnetic-electric transitions, particularly at low temperatures. Recently, some experimental prospects for the hybrid channel with thermal, magnetic, and classical dephasing parts controlled by static noise, which is used to study the dynamics of the two-qubit Heisenberg spin state as defined by various parameters such as spin-spin, DM, and KSEA interactions have been investigated [38]. Given that their model is fairly similar to ours and that it is experimentally feasible, one can presume that the model and its predictive capabilities are feasible.

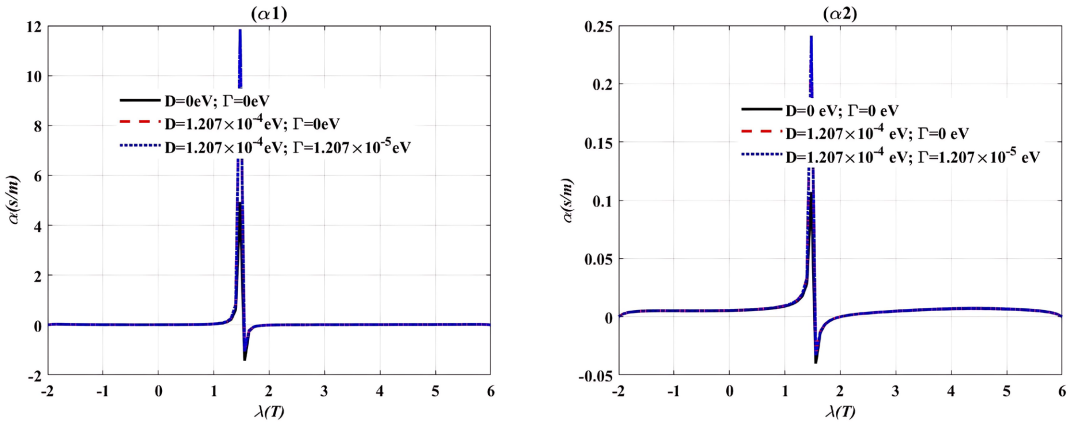

Figure 11. Magnetic field dependence's of magnetoelectric coupling factor for different values of DM and KSEA interactions, considering the Electric field intensity to be $E = 1\,\mathrm{V/m}$. ($\alpha 1$) $T = 1\,\mathrm{K}$ and ($\alpha 2$) $T = 50\,\mathrm{K}$.

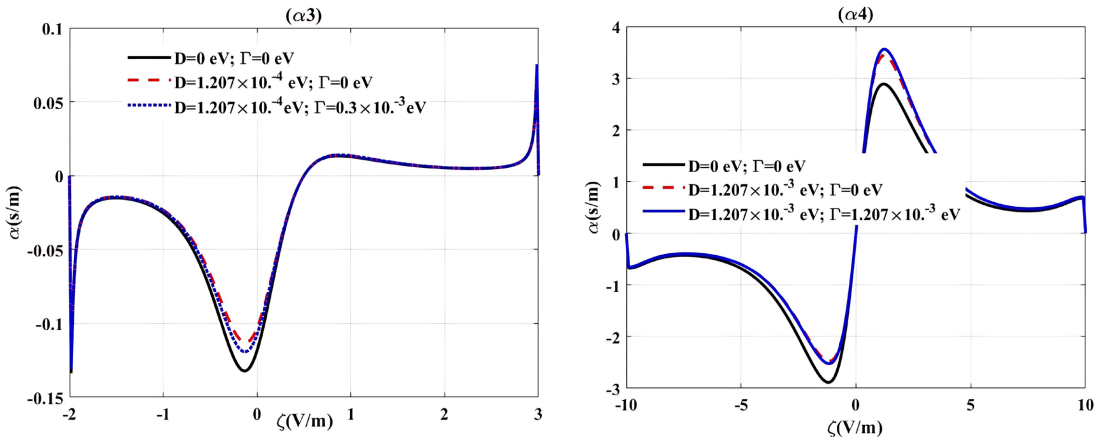

Figure 12. Electric field dependence's of magnetoelectric coupling factor for different values of DM and KSEA interactions, considering the electric field intensity to be $\lambda = 1.5\,\mathrm{T}$. ($\alpha 3$) $T = 1\,\mathrm{K}$ and ($\alpha 4$) $T = 50\,\mathrm{K}$.

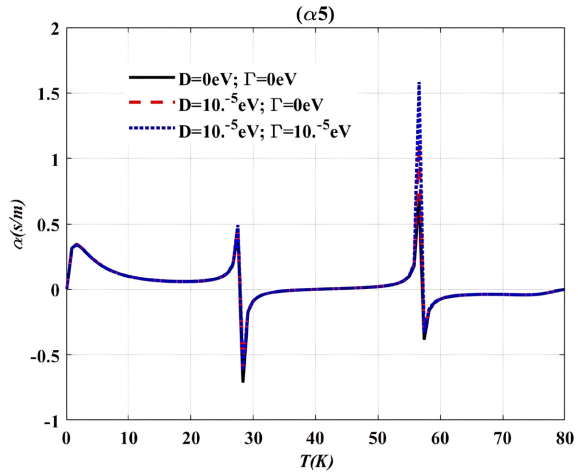

Figure 13. Temperature dependence's of magnetoelectric coupling factor for different values of DM and KSEA interactions. The other parameters are $\lambda = 1\,\mathrm{T}$ and $E = 1\,\mathrm{V/m}$.

5. Conclusion

The purpose of this study was to investigate the simultaneous action of DM and KSEA interactions used at thermal equilibrium to control $RMnO_3$ ($TbMnO_3$) multiferroic compounds. Using a helical frustrated spin chain under the constraint of an external field, a theoretical investigation of ME coupling factor and thermodynamic properties was performed. It emerges from field scans of entropy, heat capacity, and ME coupling a set of interdependent nonlinearities, resulting in metatransitions revealed by a breakdown in the interdependence of magnetic and electric order. The time required for successive and reversed transitions at the expense of an applied external field is maintained by system expenditure in DM and KSEA interactions. This gives rise to manipulating, according to interest, the ME coupling, which is essential for the design of materials with desired functionalities. The magnitude of the thermodynamic properties (entropy and specific heat) decreases, whereas one of the ME coupling factors increases as the applied electric

field strength decreases and vice versa. The magnitude change is maintained by the simultaneous effect of DM and KSEA interactions, which favours ME coupling control in $TbMnO_3$ for designing next-generation spintronics materials.

Conflicts of Interest

The authors declare no conflicts of interest regarding the publication of this paper.

References

[1] Uhlenbeck, G.E. (1976) Fifty Years of Spin: Personal Reminiscences. *Physics Today*, **29**, 43-48. https://doi.org/10.1063/1.3023519

[2] Ohanian, H.C. (1986) What Is Spin? *American Journal of Physics*, **54**, 500-505. https://doi.org/10.1119/1.14580

[3] Fouokeng, G.C., Fodouop, F.K., Tchoffo, M., Fai, L.C. and Randrianantoandro, N. (2018) "Metamagnetoelectric" Effect in Multiferroics. *Journal of Magnetism and Magnetic Materials*, **453**, 118-124. https://doi.org/10.1016/j.jmmm.2017.12.104

[4] Xu, Y. (2013) Ferroelectric Materials and Their Applications. Elsevier.

[5] Fodouop, F.K., Fouokeng, G.C., Tchoffo, M., Fai, L.C. and Randrianantoandro, N. (2019) Thermodynamics of Metamagnetoelectric Effect in Multiferroics. *Journal of Magnetism and Magnetic Materials*, **474**, 456-461. https://doi.org/10.1016/j.jmmm.2018.10.080

[6] Salje, E.K.H. (2012) Ferroelastic Materials. *Annual Review of Materials Research*, **42**, 265-283. https://doi.org/10.1146/annurev-matsci-070511-155022

[7] Smolenskiĭ, G.A. and Chupis, I.E. (1982) Ferroelectromagnets. *Soviet Physics Uspekhi*, **25**, 475-493. https://doi.org/10.1070/pu1982v025n07abeh004570

[8] Schmid, H. (1994) Multi-Ferroic Magnetoelectrics. *Ferroelectrics*, **162**, 317-338. https://doi.org/10.1080/00150199408245120

[9] Harris, A.B., Kenzelmann, M., Aharony, A. and Entin-Wohlman, O. (2008) Effect of Inversion Symmetry on the Incommensurate Order in Multiferroic $R\,Mn_2O_5$(R = Rare Earth). *Physical Review B*, **78**, Article ID: 014407. https://doi.org/10.1103/physrevb.78.014407

[10] Zhu, J.L., Yang, H.X., Feng, S.M., Wang, L.J., Liu, Q.Q., Jin, C.Q., *et al.* (2013) The Multiferroic Properties of $Bi(Fe_{1/2}Cr_{1/2})O_3$ Compound. *International Journal of Modern Physics B*, **27**, Article ID: 1362023. https://doi.org/10.1142/s0217979213620233

[11] Li, B., Zhou, J., Li, L., Wang, X.J., Liu, X.H. and Zi, J. (2003) Ferroelectric Inverse Opals with Electrically Tunable Photonic Band Gap. *Applied Physics Letters*, **83**, 4704-4706. https://doi.org/10.1063/1.1631737

[12] Shimakawa, Y., Azuma, M. and Ichikawa, N. (2011) Multiferroic Compounds with Double-Perovskite Structures. *Materials*, **4**, 153-168. https://doi.org/10.3390/ma4010153

[13] Harris, A.B., Aharony, A. and Entin-Wohlman, O. (2008) Order Parameters and Phase Diagram of Multiferroic $R\,Mn_2O_5$. *Physical Review Letters*, **100**, Article ID: 217202. https://doi.org/10.1103/physrevlett.100.217202

[14] Kimura, T., Kawamoto, S., Yamada, I., Azuma, M., Takano, M. and Tokura, Y. (2003) Magnetocapacitance Effect in Multiferroic $BiMnO_3$. *Physical Review B*, **67**, Article ID: 180401. https://doi.org/10.1103/physrevb.67.180401

[15] Cheng, Z., Wang, X., Dou, S., Kimura, H. and Ozawa, K. (2008) Improved Ferroelectric

Properties in Multiferroic $BiFeO_3$ Thin Films through La and Nb Codoping. *Physical Review B*, **77**, Article ID: 092101. https://doi.org/10.1103/physrevb.77.092101

[16] Park, S., Choi, Y.J., Zhang, C.L. and Cheong, S. (2007) Ferroelectricity in an S = 1/2 Chain Cuprate. *Physical Review Letters*, **98**, Article ID: 057601. https://doi.org/10.1103/physrevlett.98.057601

[17] Seki, S., Yamasaki, Y., Soda, M., Matsuura, M., Hirota, K. and Tokura, Y. (2008) Correlation between Spin Helicity and an Electric Polarization Vector in Quantum-Spin Chain Magnet $LiCu_2O_2$. *Physical Review Letters*, **100**, Article ID: 127201. https://doi.org/10.1103/physrevlett.100.127201

[18] Katsura, H., Nagaosa, N. and Balatsky, A.V. (2005) Spin Current and Magnetoelectric Effect in Noncollinear Magnets. *Physical Review Letters*, **95**, Article ID: 057205. https://doi.org/10.1103/physrevlett.95.057205

[19] Smolenskii, G.A. and Bokov, V.A. (1964) Coexistence of Magnetic and Electric Ordering in Crystals. *Journal of Applied Physics*, **35**, 915-918. https://doi.org/10.1063/1.1713535

[20] Sahu, J.R., Serrao, C.R., Ray, N., Waghmare, U.V. and Rao, C.N.R. (2007) Rare Earth Chromites: A New Family of Multiferroics. *Journal of Materials Chemistry*, **17**, 42-44. https://doi.org/10.1039/b612093h

[21] Khomskii, D. (2009) Classifying Multiferroics: Mechanisms and Effects. *Physics*, **2**, Article 20. https://doi.org/10.1103/physics.2.20

[22] Tagantsev, A.K., Cross, L.E. and Fousek, J. (2010) Domains in Ferroic Crystals and Thin Films. Springer. https://doi.org/10.1007/978-1-4419-1417-0

[23] Fouokeng, G.C., Fodouop, F.K., Tchoffo, M., Fai, L.C. and Randrianantoandro, N. (2018) "Metamagnetoelectric" Effect in Multiferroics. *Journal of Magnetism and Magnetic Materials*, **453**, 118-124. https://doi.org/10.1016/j.jmmm.2017.12.104

[24] Mochizuki, M. and Furukawa, N. (2009) Microscopic Model and Phase Diagrams of the Multiferroic Perovskite Manganites. *Physical Review B*, **80**, Article ID: 134416. https://doi.org/10.1103/physrevb.80.134416

[25] Matsuda, M., Fishman, R.S., Hong, T., Lee, C.H., Ushiyama, T., Yanagisawa, Y., *et al.* (2012) Magnetic Dispersion and Anisotropy in Multiferroic $BiFeO_3$. *Physical Review Letters*, **109**, Article ID: 067205. https://doi.org/10.1103/physrevlett.109.067205

[26] Kenzelmann, M., Harris, A.B., Jonas, S., Broholm, C., Schefer, J., Kim, S.B., *et al.* (2005) Magnetic Inversion Symmetry Breaking and Ferroelectricity in $TbMnO_3$. *Physical Review Letters*, **95**, Article ID: 087206. https://doi.org/10.1103/physrevlett.95.087206

[27] Blasco, J., Ritter, C., García, J., de Teresa, J.M., Pérez-Cacho, J. and Ibarra, M.R. (2000) Structural and Magnetic Study of $Tb_{1-x}Ca_xMnO_3$ Perovskites. *Physical Review B*, **62**, 5609-5618. https://doi.org/10.1103/physrevb.62.5609

[28] Yasui, Y., Yanagisawa, Y., Okazaki, R. and Terasaki, I. (2013) Dielectric Anomaly in the Quasi-One-Dimensional Frustrated Spin-1/2 System $Rb_2(Cu_{1-x}M_x)_2Mo_3O_{12}$ (M = Ni and Zn). *Physical Review B*, **87**, Article ID: 054411. https://doi.org/10.1103/physrevb.87.054411

[29] Reynolds, N., Mannig, A., Luetkens, H., Baines, C., Goko, T., Scheuermann, R., *et al.* (2019) Magnetoelectric Coupling without Long-Range Magnetic Order in the Spin-1/2 Multiferroic $Rb_2Cu_2Mo_3O_{12}$. *Physical Review B*, **99**, Article ID: 214443. https://doi.org/10.1103/physrevb.99.214443

[30] Jia, C., Onoda, S., Nagaosa, N. and Han, J.H. (2007) Microscopic Theory of Spin-

Polarization Coupling in Multiferroic Transition Metal Oxides. *Physical Review B*, **76**, Article ID: 144424. https://doi.org/10.1103/physrevb.76.144424

[31] Arima, T., Tokunaga, A., Goto, T., Kimura, H., Noda, Y. and Tokura, Y. (2006) Collinear to Spiral Spin Transformation without Changing the Modulation Wavelength Upon Ferroelectric Transition in $Tb_{1-x}Dy_xMnO_3$. *Physical Review Letters*, **96**, Article ID: 097202. https://doi.org/10.1103/physrevlett.96.097202

[32] Jia, C. and Berakdar, J. (2011) Electric Field Effects on the Thermodynamics of Multiferroic Chains. *Journal of Superconductivity and Novel Magnetism*, **25**, 2679-2681. https://doi.org/10.1007/s10948-011-1241-2

[33] Cheong, S. and Mostovoy, M. (2007) Multiferroics: A Magnetic Twist for Ferroelectricity. *Nature Materials*, **6**, 13-20. https://doi.org/10.1038/nmat1804

[34] Fodouop, F.K., Fouokeng, G.C., Ateuafack, M.E., Tchoffo, M. and Fai, L.C. (2020) Metamagnetoelectric Effect in Multiferroics $A_2Cu_2Mo_3O_{12}$ (A = Rb and Cs) Quantum Spin Chain. *Physica B*: *Condensed Matter*, **598**, Article ID: 412455. https://doi.org/10.1016/j.physb.2020.412455

[35] Alonso, J.A., Martínez-Lope, M.J., Casais, M.T. and Fernández-Díaz, M.T. (2000) Evolution of the Jahn-Teller Distortion of MnO_6 Octahedra in $RmNo_3$ Perovskites (R = Pr, Nd, Dy, Tb, Ho, Er, Y): A Neutron Diffraction Study. *Inorganic Chemistry*, **39**, 917-923. https://doi.org/10.1021/ic990921e

[36] Tchoffo, M., Fodouop, F.K., Fouokeng, G.C., Randrianantoandro, N. and Fai, L.C. (2019) Temperature-Dependent Interplay of Anisotropic Exchange Coupling and External Fields on Metamagnetoelectric Multiferroics. *Materials Research Express*, **6**, Article ID: 096102. https://doi.org/10.1088/2053-1591/ab2a64

[37] Vopson, M.M. (2015) Fundamentals of Multiferroic Materials and Their Possible Applications. *Critical Reviews in Solid State and Materials Sciences*, **40**, 223-250. https://doi.org/10.1080/10408436.2014.992584

[38] Rahman, A.U., Yang, M., Zangi, S.M. and Qiao, C. (2023) Probing a Hybrid Channel for the Dynamics of Non-Local Features. *Symmetry*, **15**, Article 2189. https://doi.org/10.3390/sym15122189